INDEX COPERNICUS INTERNATIONAL

Bio-Algorithms and Med-Systems

WWW.BAMSJOURNAL.COM ISSN: 1896-530X

ORIGINAL ARTICLE

Received: 11.12.2025
Accepted: 30.12.2025
Published: 31.12.2025

CITE THIS ARTICLE AS:
Moyo S, Stepien E, Moskal P, "Characterisation of Plasma Blood Clots in Different Physical States Using Positron Annihilation Lifetime Spectroscopy," Bio-Algorithms and Med-Systems vol. 21, no. 1, pp. 137-145, 2025, DOI: 10.5604/01.3001.0055.5409

AUTHORS' CONTRIBUTION:
A – Conceptualization
B – Data Curation
C – Formal Analysis
D – Funding Acquisition
E – Investigation
F – Methodology
G – Project Administration
H – Resources
I – Software
J – Supervision
K – Validation
L – Visualization
M – Writing – Original Draft
N – Writing – Review & Editing

CORRESPONDING AUTHOR:
Ewa Stępień; Faculty of Physics, Astronomy and Applied Computer Science, Jagiellonian University in Kraków, Poland; E-mail: e.stepien@uj.edu.pl

Characterisation of Plasma Blood Clots in Different Physical States Using Positron Annihilation Lifetime Spectroscopy

Simbarashe Moyo[1ABCEFKLMN], Ewa Stępień[1ADFGJKN], Paweł Moskal[1ADFGJKN]

[1]Faculty of Physics, Astronomy and Applied Computer Science, Jagiellonian University in Kraków, Poland

ABSTRACT

Objective: To quantitatively assess how different preparation methods alter the nanoscale free-volume architecture of human plasma blood clots using positron annihilation lifetime spectroscopy (PALS), and to establish the relevance of PALS for fibrin network characterisation in biomedical research.
Materials: Human plasma blood clots prepared in four distinct physical states: fresh, glutaraldehyde-fixed, desiccator-dried and critical-point-dried (CPD).
Methods: High-resolution fast-coincidence PALS measurements were performed at 37°C. Ortho-positronium (o-Ps) lifetimes and intensities were extracted using PALS Avalanche and independently verified by fitting in the Origin software package. Reported values represent mean ± SD from n = 3 independent plasma clots prepared and measured under identical conditions. Comparative analysis across preparation states was conducted to assess preparation-dependent variations in o-Ps parameters.
Results: Distinct o-Ps lifetime (τ_3) and intensity (I_3) values were observed across clot states: fresh (1.95 ± 0.01 ns; 11 ± 0.07%), fixed (2.11 ± 0.02 ns; 16 ± 0.16%), desiccator-dried (2.15 ± 0.04 ns; 6 ± 0.11%), and CPD (1.95 ± 0.01 ns; 9 ± 0.07%). These differences indicate that preparation protocols substantially affect positronium (Ps) lifetime characteristics and formation probability within plasma clots.
Conclusions: Sample preparation has a pronounced effect on PALS-derived o-Ps parameters in plasma blood clots, underscoring the sensitivity of PALS to preparation-induced nanoscale changes. To the best of our knowledge, this study provides the first systematic PALS-based comparison of plasma clots across multiple physical states, highlighting the importance of protocol selection when applying positronium-based techniques to biological materials.

KEYWORDS

positron annihilation lifetime spectroscopy, fibrin fibres, fibrin network, nanostructure

LIST OF ABBREVIATIONS

CPD – critical-point-dried
DFP – Davidon–Fletcher–Powell
FWHM – Full Width at Half Maximum
J-PET – Jagiellonian-positron emission tomography
o-Ps – ortho-positronium
PALS – positron annihilation lifetime spectroscopy
PET – positron emission tomography
PPP – platelet-poor plasma
p-Ps – para-positronium
Ps – positronium
SEM – scanning electron microscopy

BRIEF DESCRIPTION OF THE WORK

This study shows that nanoscale structural differences in blood clots critical for understanding thrombosis and treatment response can be quantitatively detected using positron annihilation lifetime spectroscopy (PALS). By revealing how common preparation methods alter fibrin architecture, the work advances the development of reliable nanoscale biomarkers for future diagnostic and clinical imaging applications.

INTRODUCTION

Blood clot formation is a fundamental biological mechanism that maintains haemostasis and prevents excessive bleeding following vascular injury. Central to this process is fibrin, the structural protein that polymerises into an intricate three-dimensional network providing the clot with mechanical strength and stability. The architecture of this fibrin network, including fibre thickness, branching, density, porosity and interconnectivity, plays a decisive role in determining clot stability, mechanical behaviour and susceptibility to fibrinolysis [1–7]. Variations in these micro- and nanoscale structural features influence clot deformation, fluid transport and enzymatic degradation, underscoring the importance of fibrin network organisation in both physiological coagulation and thrombotic disease.

Alterations in fibrin network structure have been implicated in pathological conditions such as venous thromboembolism, cardiovascular disease and impaired fibrinolysis. Studies by Undas, Stępień and collaborators have demonstrated that biochemical and clinical factors, including dyslipidaemia, inflammation, and inherited coagulation abnormalities can modify fibrin density and pore architecture, resulting in stiffer, less permeable clots that are more resistant to lysis [1, 8, 9]. These findings highlight the need for analytical techniques capable of resolving nanoscale structural differences within fibrin matrices.

PALS is a powerful, non-destructive technique widely applied to investigate free-volume and nanoscale voids in polymers, semiconductors and biological materials [10, 11]. PALS is uniquely sensitive to sub-nanometre to nanometre-sized free-volume regions through the measurement of positronium (Ps) lifetimes. Ps exists as either para-positronium (p-Ps), with a vacuum lifetime of 0.125 ns, or ortho-positronium (o-Ps), which exhibits a much longer intrinsic lifetime of 142 ns [12]. In condensed matter, o-Ps becomes trapped in regions of low electron density, where pickoff annihilation reduces its lifetime in proportion to local free-volume dimensions [13, 14]. This makes PALS ideally suited for probing nanoscale voids within fibrin networks.

Beyond materials science, recent breakthroughs have demonstrated the potential of Ps measurements for biomedical and clinical imaging. Moskal and collaborators have shown that total-body positron emission tomography (PET) systems can detect Ps-related signals in vivo, enabling nanoscale characterisation of tissue microstructure [10], and Ps has emerged as a promising biomarker for disease detection and tissue characterisation [15, 16]. Proof-of-concept studies by Moyo, Moskal and Stępień have demonstrated that PALS can distinguish fibrin clots of different biological origins [17], while recent subsequent work extended Ps-based imaging to cardiac tumours, enabling simultaneous acquisition of PET and Ps-specific parameters [18]. Additional studies have shown that PALS parameters differentiate healthy and neoplastic tissues [19] and can characterise lipid membranes, vesicles, and skin barrier structures [20–22].

Despite these advances, the influence of sample preparation protocols on PALS measurements of biological tissues remains insufficiently characterised. Common preparation methods such as chemical fixation, dehydration or critical-point-dried (CPD) can alter water content, protein conformation and network architecture, thereby changing nanoscale free-volume distributions [23, 24]. Glutaraldehyde fixation stabilises fibrin structure through covalent cross-linking and may preserve or modify native pore geometry [25]. In contrast, dehydration techniques variably preserve ultrastructure and can induce structural compaction due to surface tension effects during drying [26]. Such preparation-induced changes may significantly affect measured Ps lifetimes and intensities, complicating the interpretation of PALS data obtained from biological samples [27, 28].

Understanding how fibrin network structure relates to clot function is essential in thrombosis research [5]. Fibrin clots exhibit diverse architectures depending on fibrinogen and thrombin concentrations, ionic conditions, pH and the presence of blood cells [29, 30]. Low-thrombin clots typically form thick, loosely connected fibres with high permeability and rapid fibrinolysis, whereas high-thrombin conditions favour thin, densely packed networks that are more resistant to degradation [29, 31–33]. Clot mechanical properties, including stiffness, elasticity and rupture resistance, are governed by fibre diameter, protofibril packing and pore organisation [31, 34, 35]. Altered fibrin network characteristics have been linked to pathological states such as thrombosis, embolism and coagulopathy [1, 5–7, 9, 36–38].

Given the sensitivity of PALS to nanoscale free-volume environments and the complexity of fibrin architecture, it is essential

to clarify how preparation protocols influence PALS-derived parameters. The primary aim of this study is methodological: to systematically assess how different preparation states, fresh, chemically fixed, desiccator-dried and CPD, affect o-Ps lifetimes and intensities in plasma blood clots. We hypothesise that each preparation method produces a distinct Ps signature reflecting preparation-induced modifications of the nanoscale free-volume environment. By comparing PALS parameters across these four physical states, this work evaluates the impact of fixation and dehydration on nanoscale measurements and, to the best of our knowledge, provides a systematic assessment of preparation effects in fibrin-based materials.

MATERIALS AND METHODS

Preparation of Plasma Blood Clots in Different Physical States

Fresh plasma blood clots were prepared using platelet-poor plasma obtained from the Regional Centre for Blood Donation and Blood Treatment in Kraków. Plasma was obtained from three independent human donors, and all reported measurements corresponding to n = 3 independent plasma clots, each prepared from a separate plasma aliquot under identical conditions. The plasma was first separated from red blood cells by centrifugation and then thawed. To induce clot formation, calcium chloride and thrombin were added to the plasma, and the mixture was incubated at 37°C until clotting occurred. All clots were prepared using identical plasma volumes (500–1000 µL) and within identical cylindrical geometries defined by the preparation wells. Once formed, the clot was gently separated from the serum using a sterile spatula and washed three times with Tris-HCl buffer (pH 7.4) to remove residual serum components. Fresh clots were measured by PALS within 1 hour of preparation, following a brief equilibration period at 37°C. Fig. 1. illustrates each step in the preparation of the four clot states analysed in this study.

To preserve clot structure, a fixation solution was prepared by mixing 1 mL of 2.5% glutaraldehyde with 4 mL of Tris-HCl buffer. The plasma clot was submerged in this fixative and left to incubate at room temperature for 24 hours. The previously stated 30–60-minute interval corresponds to preliminary optimisation experiments; all samples reported in this study were fixed for 24 hours to ensure complete cross-linking and methodological consistency. After incubation, the clot was removed and washed thoroughly with fresh Tris-HCl buffer to eliminate any residual glutaraldehyde, ensuring compatibility with subsequent analyses, such as PALS or imaging.

For desiccator drying, clots were placed on sterile glass slides and transferred into a vacuum desiccator containing activated anhydrous calcium sulphate as the desiccant. The desiccator maintained a relative humidity of approximately 2%. Initial clot

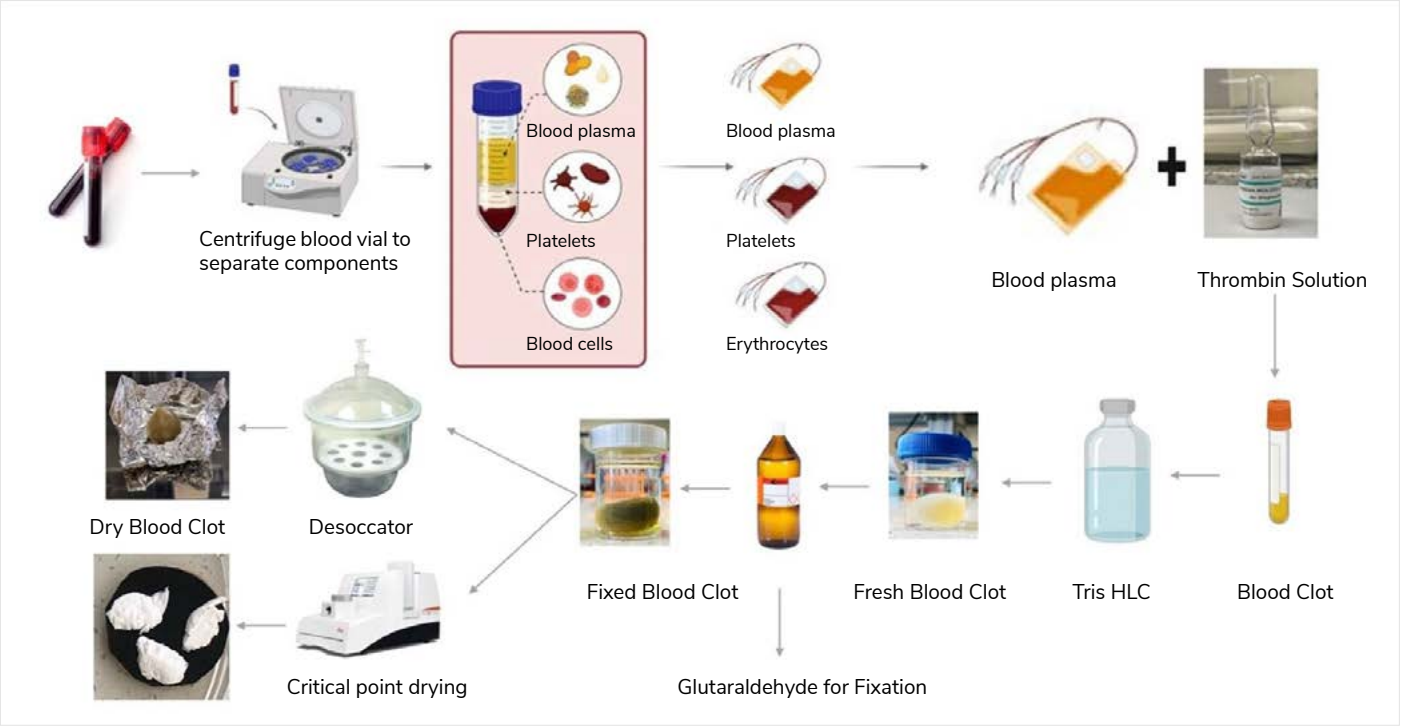

Fig. 1. Preparation workflow for fresh, fixed, desiccator-dried and CPD plasma blood clots. Platelet-poor plasma (PPP) was obtained by centrifuging whole blood at 2500 × g for 15 minutes. Thawed PPP (500–1000 µL) was mixed with a thrombin working solution (final activity 1–2 U/mL) in 50 mM Tris–HCl buffer (pH 7.4), supplemented with $CaCl_2$ (final concentration 10–20 mM), and incubated at 37°C for 30–45 minutes to form clots. Fresh clots were washed three times with Tris-HCl buffer. Fixed clots were treated with 2.5% glutaraldehyde for 24 hours. Dried clots were obtained either by desiccator drying or critical-point drying following ethanol dehydration.

weights were recorded to monitor dehydration progress, and the clots were left to dry for four days. The four-day drying period was selected based on mass stabilisation, defined as less than 1% change in mass over 24 hours, indicating completion of dehydration. Afterward, they were gently removed for further structural or spectroscopic evaluation.

The CPD technique was used to preserve the ultrastructure of plasma clots, especially for scanning electron microscopy (SEM). Clots were first fixed in 4% paraformaldehyde and then dehydrated through a graded ethanol series (50%, 60%, 70%, 80%, 90%, 99% and 100%), with each step lasting 30 minutes. Following dehydration, the clots were transferred into a CPD chamber, where ethanol was replaced with liquid CO_2. The drying process occurred at 31°C and 74 bar, the critical point of CO_2, allowing the sample to dry without structural collapse due to surface tension. CPD--treated clots were measured by PALS immediately after drying, without additional storage or equilibration.

All four clot preparation methods – fresh, fixed, desiccator dried and critically dried – are illustrated in Fig. 2., which provides a visual comparison of the physical states analysed in this study.

PALS Setup

PALS measurements were conducted using a high-resolution two-detector fast-coincidence system. Clots in each preparation state were bisected and positioned symmetrically around a ^{22}Na positron source inside a custom aluminium chamber with paired 200 µL cavities. Measurements were performed at 37°C to mimic physiological conditions. Temperature stability was maintained within ± 0.5°C using a thermostated sample holder. The ^{22}Na source, encapsulated in thin Kapton foil, provided the 1274 keV prompt γ-ray for lifetime start timing and the ensuing 511 keV annihilation photons for stop signals.

Detection used two BaF2 scintillators coupled to Hamamatsu H3378-51 PMTs [39]. The system recorded the 1274 keV prompt photon and 511 keV annihilation photons with high temporal resolution. Constant fraction discriminators improved time pickoff, and timing signals were digitised with a DRS4-based waveform digitiser [40] for sub-nanosecond timing resolution. Coincidence logic synchronised events and data were collected and monitored on a dedicated acquisition computer [39, 40]. The overall time resolution of the system was approximately 230 ps Full Width at Half Maximum (FWHM). Each spectrum contained (2–4) × 10^6 counts, and identical acquisition times were used for all samples. Background measurements using a source-only configuration were performed and treated as a constant offset during fitting.

All measurements were conducted under ambient laboratory atmosphere; humidity was not actively controlled but remained stable during acquisition.

Lifetime Spectrum Analysis

The acquired PALS spectra were analysed using the PALS Avalanche software package developed by Kamil Dulski and collaborators within the Jagiellonian-positron emission tomography (J-PET) project [41]. This ROOT-based C++ framework is optimised for multicomponent decomposition of complex lifetime spectra and performs the fit by convolving exponential decay components with the detector's Gaussian time-resolution function.

This approach enables stable extraction of p-Ps and o-Ps lifetime components even in heterogeneous biological samples. In addition, the Ps lifetimes were independently determined using Origin software (OriginLab, Northampton, MA) by fitting the experimental data with a composite model comprising a superposition of convolutions between Gaussian and exponential functions, expressed as:

$$y = y_0 + f(x) * h(x) = y_0 + \sum_{i=1}^{4} \frac{A_i}{t_i} e^{-\left(\frac{x}{t_i}\right)} e^{-\frac{(x-x_c)}{t_i}} \int_{-\infty}^{z_i} \frac{1}{\sqrt{2\pi}} e^{-\frac{\tau^2}{2}} d\tau$$

Where:

$$f(x) = \sum_{i=1}^{4} \frac{A_i}{t_i} e^{-\frac{x}{t_i}}, h(x) = \frac{1}{\sqrt{2\pi}w} e^{-\frac{(x-x_c)^2}{w^2}}, z_i = \frac{x - x_c}{w} - \frac{w}{t_i}$$

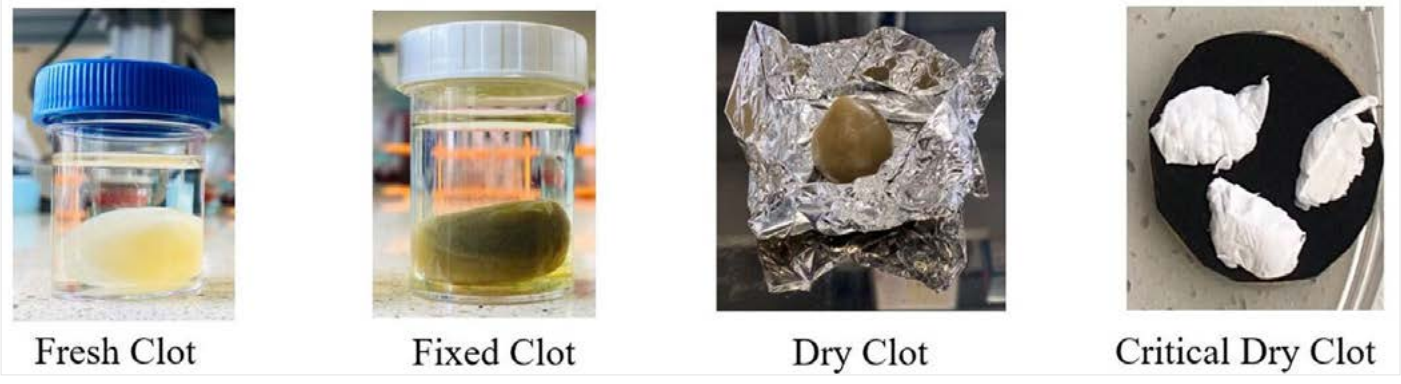

Fig. 2. Representative pictures showing different types of plasma blood clots used in this study: fresh, chemically fixed with glutaraldehyde, desiccator-dried and critical point dried. The images illustrate the macroscopic appearance of clots in each physical state.

Tab. I. Summary of positron annihilation components, their characteristic lifetimes and fitting constraints. Fixed components were constrained according to literature values.

COMPONENT	LIFETIME (ns)	INTENSITY (%)	ACTION	COLOUR CODE
p-Ps intrinsic [8]	0.125	0.045	Fixed	Green
Kapton foil (source encapsulation) [33]	0.386	0.10	Fixed	Yellow
Aluminum chamber [34, 35]	0.166	0.25	Lifetime Fixed	Dark Green
Air gap (interfacial free positron) [8, 36]	0.210	0.10	Lifetime Fixed	Blue Green
Direct annihilation (non-Ps positrons)	0.500	0.30	Not Fixed	Turquoise / Cyan
o-Ps in sample (free volume)	2.000	0.15	Not Fixed	Blue

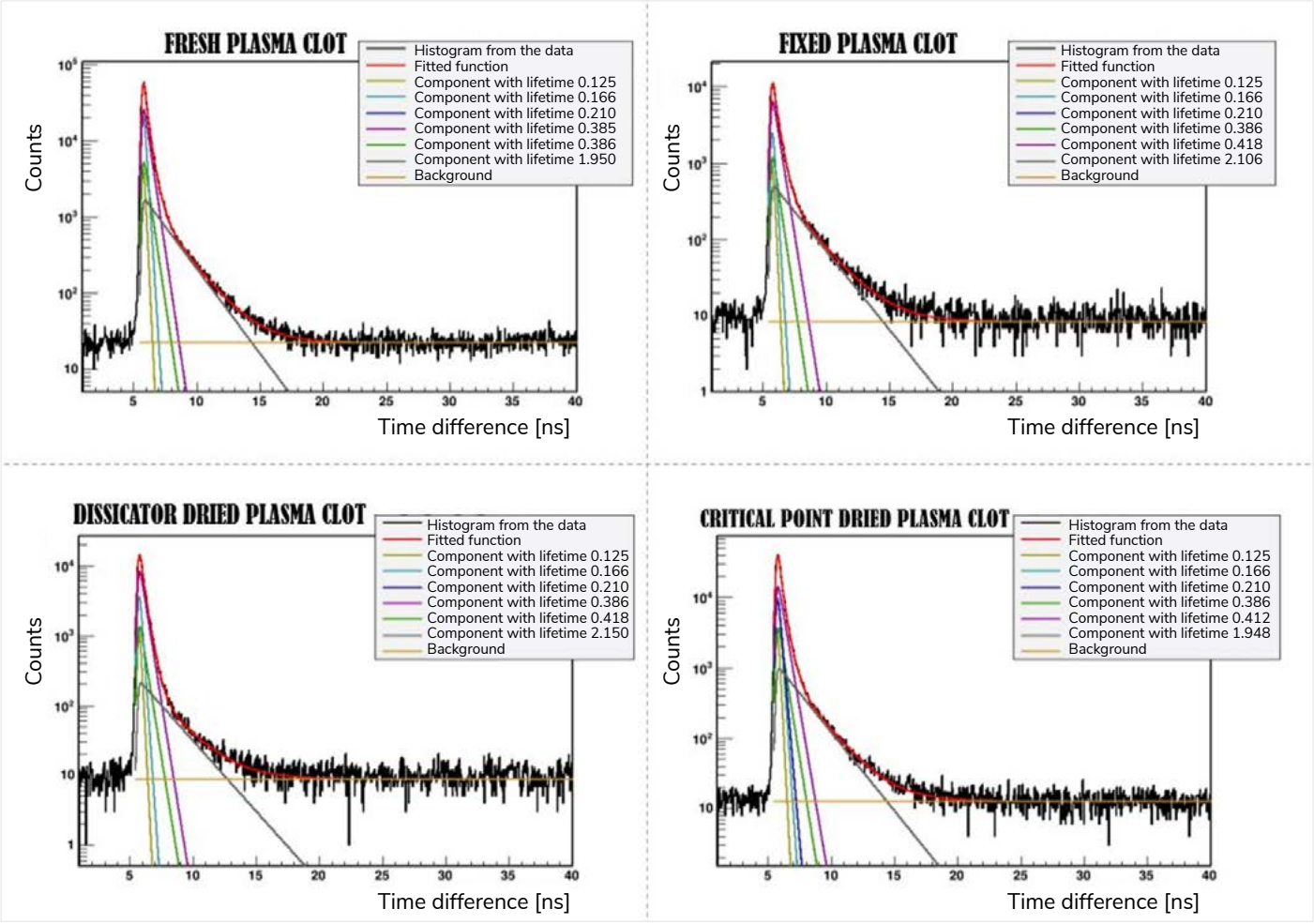

Fig. 3. A combined spectrum of Ps lifetimes for fresh, fixed, desiccator-dried and critical-point dried plasma clots is shown in the extended scale. The black histogram represents the measured data, while the **red** curve shows the fitted multicomponent decay function. The superimposed coloured lines indicate the distributions of individual components: **green** corresponds to intrinsic p-Ps ($\tau \approx 0.125$ ns), which is fully fixed; **yellow** denotes annihilations in the Kapton source material ($\tau \approx 0.386$ ns), also fully fixed; **dark green** represents annihilations in the aluminium chamber ($\tau \approx 0.166$ ns), with lifetime fixed; **blue-green** corresponds to the air-gap/interfacial component ($\tau \approx 0.210$ ns), also lifetime-fixed; **turquoise** represents direct free--positron annihilation which is not fixed showing the following results, 0.39 ns (fresh clot), 0.42 ns (fixed), 0.39 ns (desiccator-dried clot) and 0.41 ns (critical-point dried clot); blue indicates the long-lived o-Ps component associated with nanoscale free volumes, with the following results: 1.95 ns (fresh clot), 2.11 ns (fixed clot), 2.15 ns (desiccator-dried clot) and 1.94 ns (critical-point dried clot); purple denotes the background; and red represents the total fitted multicomponent function.

Here, y_0 denotes the constant background, A_i represents the area of the i^{th} convolution component, w is the standard deviation of the Gaussian resolution function, x_c is the offset position of the instrumental response and t_i corresponds to the Ps lifetime of the i^{th} exponential component [41].

In PALS Avalanche, the experimental spectrum is modelled as a weighted sum of exponential decay components corresponding to different annihilation environments, each convolved with the detector-resolution function. The background was treated as a constant offset, and the Gaussian resolution parameters were

determined directly during the fitting procedure. Initial fitting parameters for nonfixed components were selected based on prior literature values and preliminary unconstrained fits, and identical fitting constraints were applied consistently across all samples. Parameter minimisation was performed using the Minuit package via the Davidon–Fletcher–Powell (DFP) algorithm [41].

Fitting stability was assessed by the inspection of residuals, consistency of extracted parameters across repeated fits and evaluation of parameter correlations, in addition to reduced χ^2 values. To stabilise the fits and ensure the accurate separation of overlapping components, several short-lived annihilation components were fixed to well--established literature values. These fixed parameters correspond to annihilation occurring in materials external to the biological sample (e.g., Kapton source foil, aluminium window, air) and are summarised in Tab. I. Fixing these components improves the robustness of the extraction of the biologically relevant p-Ps and o-Ps lifetimes.

RESULTS

Lifetime Spectra Analysis

Representative positron lifetime spectra for each clot preparation state are shown in Fig. 3. Experimental data (black histograms) are overlaid with multicomponent decay fits. Each spectrum contained (2–4) × 10^6 total counts, ensuring reliable multicomponent decomposition. Fit quality was evaluated using reduced chi-squared values (χ^2/ν), which are expected to lie close to unity (typically 1.0b ± 0.2) for a well-resolved PALS spectrum [42]. The obtained values, 1.2474 (fresh), 1.1839 (fixed), 1.1648 (desiccator-dried) and 1.2454 (CPD), all fall within this accepted range, confirming excellent agreement between the fitted model and the experimental data.

The lifetime spectra reveal preparation-dependent differences in the relative contributions of τ_2 and τ_3 components across the four clot states. Quantitative values extracted for these components are summarised in Tab. II.

Ps Lifetime Measurements showing Non-Fixed (free) Components

The Ps lifetime measurements obtained for plasma blood clots in four different physical states are summarised in Tab. II. All measurements were performed at 37°C. Reported values represent mean ± standard deviation derived from n = 3 independent plasma clots. The standard deviations primarily reflect variability between independently prepared clots rather than those fitting uncertainty.

The lifetime spectra were modelled using multiple exponential components corresponding to distinct annihilation processes [43]. The shortest component (τ_1 = 0.125 ns) [12, 44] was assigned to p-Ps decay, and its intensity (I_1) was fixed at 5% for all samples to stabilise fits and reduce parameter correlations, consistent with prior PALS studies of hydrated biological materials. The intermediate component τ_2 (≈0.39–0.42 ns) corresponds to free--positron and pickoff annihilation processes and is treated here as a mixed, nonspecific component rather than a direct structural descriptor. The longest-lived component τ_3 is attributed to o-Ps annihilation in nanoscale free-volume environments.

Fresh clots exhibited τ_2 = 0.39 ± 0.001 ns with an intensity of 49 ± 0.07%, and τ_3 = 1.95 ± 0.01 ns with an intensity of 11 ± 0.07%. Fixed clots showed increased τ_2 and τ_3 lifetimes (0.42 ± 0.002 ns and 2.11 ± 0.02 ns, respectively), accompanied by higher τ_2 and τ_3 intensities. Desiccator-dried clots exhibited τ_2 = 0.39 ± 0.002 ns with the highest τ_2 intensity (62 ± 0.11%), while τ_3 increased to 2.15 ± 0.04 ns with a markedly reduced intensity of 6 ± 0.11%. CPD-treated clots showed intermediate values for both τ_2 and τ_3 components.

DISCUSSION

PALS measurements revealed that plasma clot nanostructure is strongly modulated by preparation method. Fresh clots exhibited moderate o-Ps lifetimes and low intensities, consistent with hydrated nanoscale free-volume environments within the fibrin network, and with known effects of water on protein packing and Ps formation [45]. Fixation with glutaraldehyde increased both o-Ps lifetime and intensity, reflecting stabilisation of fibrin architecture through covalent cross-linking and associated modifications of the average free-volume environment, rather than a direct change in pore size [46, 47]. Desiccator drying produced the longest τ_3 values but markedly reduced intensities, a combination characteristic of dehydration-induced compaction and chemical quenching effects that reduce Ps formation probability, commonly observed in dried biological materials [48]. Critical-point drying generated intermediate o-Ps parameters, consistent with partial preservation of nanoscale free-volume

Tab. II. Ps lifetime parameters for plasma blood clots in different physical states measured at 37°C. Values represent mean ± standard deviation (n = 3).

BLOOD CLOT	TEMP.	SAMPLE ID	T_1 [ns]	I_1 [%]	T_2 [ns]	I_2 [%]	T_3 [ns]	I_3 [%]
Fresh Clot	37°C	FRBCLOT	0.125	5	0.39 ± 0.001	49 ± 0.07	1.95 ± 0.01	11 ± 0.07
Fixed Clot	37°C	FXDBCLOT	0.125	5	0.42 ± 0.002	56 ± 0.16	2.11 ± 0.02	16 ± 0.16
Dry Clot	37°C	DRYBC	0.125	5	0.39 ± 0.002	62 ± 0.11	2.15 ± 0.04	6 ± 0.11
CriDry Clot	37°C	CDryBC	0.125	5	0.41 ± 0.002	40 ± 0.07	1.95 ± 0.01	9 ± 0.07

Note: τ_1 = para-positronium (p-Ps) lifetime; I_1 = p-Ps intensity; τ_2 = free-positron or pickoff annihilation lifetime; I_2; τ_3 = ortho-positronium (o-Ps) lifetime; I_3 = o-Ps intensity.

environments through the elimination of surface-tension-driven collapse during drying [49].

These nanoscale alterations correspond to the multilevel architecture of fibrin networks, which consist of protofibrils bundled into fibres that branch to form a porous, three-dimensional matrix [3, 30, 50]. The τ_3 lifetimes observed here (≈2 ns) reflect average free-volume environments at the sub-nanometre scale, as described by the Tao–Eldrup model, rather than discrete pore sizes or network connectivity [13, 14].

The observed τ_3 differences between preparation states (≈0.2 ns) fall within the sensitivity range of PALS for heterogeneous biological and soft-matter systems and reflect changes in average nanoscale free-volume environments, rather than direct measurements of pore size distributions, connectivity, or network functionality [13, 14, 23, 43]. According to established Ps models, τ_3 represents an ensemble-averaged free-volume parameter governed by Ps pickoff annihilation in regions of reduced electron density [13, 14].

Similarly, variations in I_3 represent changes in Ps formation probability, which depends not only on the availability of free volume but also on the chemical composition, presence of quenching species and hydration state of the material [11, 23, 44].

Consequently, changes in I_3 should be interpreted cautiously, particularly in dehydrated or chemically modified biological samples. No formal inferential statistical testing was performed due to the limited sample size and the primarily methodological focus of this study; therefore, all reported differences should be interpreted descriptively rather than as statistically significant. Overall, within the present dataset, τ_3 was more sensitive to preparation-induced modifications of the nanoscale free--volume environment, whereas I_3 showed stronger dependence on dehydration and chemical modification.

The nanostructural differences detected by PALS should not be interpreted as direct predictors of clot permeability or fibrinolysis. Clot permeability and susceptibility to fibrinolysis are governed primarily by micron-scale fibrin architecture, fibre thickness and network connectivity [32, 36, 51, 52]. However, nanoscale free--volume properties may indirectly influence mechanical behaviour and molecular interactions within fibrin fibres, particularly under deformation, by modulating local packing density and intermolecular mobility.

At the molecular level, fibrin exhibits complex nanomechanical behaviour, with elasticity and extensibility governed by conformational rearrangements within fibrin monomers and protofibrils at length scales on the order of 10^{-8} m^2 [2, 31, 53, 54]. During the deformation of fibrin polymers, secondary structural transitions have been observed, including α-helix–to–β-sheet conversion detected using Fourier-transform infrared spectroscopy and Congo red staining [55, 56]. Such subtle nanoscale and molecular-scale rearrangements may influence local free-volume environments and, in principle, be detectable by PALS, providing complementary information to spectroscopic and mechanical techniques.

Reduced free volume in dehydrated clots corresponds to increased stiffness and decreased molecular transport, consistent with the behaviour of dried biological tissues [48, 57]. Preservation of nanoscale free-volume environments in fixed and CPD clots suggests improved retention of native-like structural features, supporting the use of these preparation methods for imaging and nanoscale characterisation where maintenance of ultrastructure is critical [49].

COMPARISON WITH PREVIOUS PALS STUDIES

The present findings are consistent with and extend previous PALS investigations of biological tissues. Moyo et al. demonstrated the feasibility of using PALS to characterise fibrin clots and showed that o-Ps lifetimes differ between various clot types [17]. This study extends work on the systematic analysis of the impact of various preparation protocols on structural measurements of biological samples [24]. The use of PALS provides a more comprehensive understanding of the physicochemical phenomena occurring in biological samples during preparation, which determine Ps lifetime in fibrin networks.

CONCLUSIONS

This study demonstrates the high sensitivity of PALS to preparation-induced nanoscale changes in plasma blood clots. By comparing fresh, glutaraldehyde-fixed, desiccator-dried and CPD clots, we show that variations in o-Ps lifetimes and intensities are strongly influenced by sample preparation protocols, reflecting changes in average free-volume environments, hydration state, and chemical modification, rather than direct measures of fibrin pore size or network connectivity. The clear distinctions observed across preparation methods highlight that sample handling is a critical methodological factor that must be carefully controlled when applying PALS to biological tissues.

Overall, these results establish the methodological value of PALS as a quantitative tool for probing nanoscale free-volume characteristics in fibrin-based biomaterials and underscore the importance of protocol selection for ensuring meaningful and reproducible measurements. By systematically assessing preparation effects, this work provides a reference framework for future PALS studies of biological samples. Extending this approach to pathological clots and integrating PALS with complementary structural and imaging techniques may further enhance nanoscale characterisation of clot microstructure and support the continued development of Ps-based approaches in biomedical research.

ACKNOWLEDGEMENTS

The authors gratefully acknowledge Drs. Karol Kubat and Jakub Dymek for their valuable assistance in sample preparation and measurements.

FUNDING

This study was supported by the National Science Centre of Poland through grants 2021/42/A/ST2/00423, 2021/43/B/ST2/02150 and 2022/47/I/NZ7/03112, as well as by the SciMat and qLife Priority Research Areas under the Excellence Initiative – Research University program at Jagiellonian University and a grant No. SPUB/SP/627733/2025 by Ministry of Science and Higher Education.

S. Moyo also acknowledges support from Jagiellonian University through DSC grant N17/MNS/RMS/21/MS/2021.

CONFLICT OF INTEREST

P. Moskal holds patents for positronium imaging. Other co-authors have no financial interests or relationships to disclose in relation to the subject of this presentation.

DATA AVAILABILITY

Data are avoilable in Rodbuk UJ (https://uj.rodbuk.pl/) repository: https://doi.org/10.57903/UJ/FLAT1N.

REFERENCES

1. Stępień E, Plicner D, Kapelak B, Wypasek E, Sadowski J, Undas A. Factor XIII Val34Leu polymorphism as a modulator of fibrin clot permeability and resistance to lysis in patients with severe coronary artery disease. Kardiol Pol. 2009;67(8):947–55.
2. Weisel JW. Structure of fibrin: Impact on clot stability. J Thromb Haemost. 2007;5(SUPPL. 1):116–24. doi: https://doi.org/10.1111/j.1538-7836.2007.02504.x
3. Collet J-P, Moen JL, Veklich YI, Gorkun OV, Lord ST, Montalescot G, et al. The αC domains of fibrinogen affect the structure of the fibrin clot, its physical properties, and its susceptibility to fibrinolysis. Blood. 2005;106(12):3824–30. doi: https://doi.org/10.1182/blood-2005-05-2150.
4. Pretorius E. Quantifying Changes in Fibrin Fiber Network Morphology. 2011;35(4):150–4. doi: https://doi.org/10.3109/01913123.2011.562622.
5. Stepień E, Kabłak-Ziembicka A, Musiałek P, Tylko G, Przewłocki T. Fibrinogen and carotid intima media thickness determine fibrin density in different atherosclerosis extents. Int J Cardiol. 2012;157(3):411–3. doi: https://doi.org/10.1016/j.ijcard.2012.03.140.
6. Undas A, Podolec P, Zawilska K, Pieculewicz M, Jedliński I, Stępień E, et al. Altered fibrin clot structure/function in patients with cryptogenic ischemic stroke. Stroke. 2009;40(4):1499–501. doi: https://doi.org/10.1161/STROKEAHA.108.532812.
7. Undas A, Wiek I, Stępień E, Zmudka K, Tracz W. Hyperglycemia is associated with enhanced thrombin formation, platelet activation, and fibrin clot resistance to lysis in patients with acute coronary syndrome. Diabetes Care. 2008;31(8):1590–5. doi: https://doi.org/10.2337/dc08-0282.
8. Undas A, Stepien E, Tracz W, Szczeklik A. Lipoprotein(a) as a modifier of fibrin clot permeability and susceptibility to lysis. J Thromb Haemost. 2006;4(5):973–5. doi: https://doi.org/10.1111/j.1538-7836.2006.01903.x.
9. Undas A, Zawilska K, Cieśla-Dul M, Lehmann-Kopydłowska A, Skubiszak A, Ciepłuch K, et al. Altered fibrin clot structure/function in patients with idiopathic venous thromboembolism and in their relatives. Blood. 2009;114(19):4272–8. doi: https://doi.org/10.1182/blood-2009-05-222380.
10. Moskal P, Dulski K, Chug N, Curceanu C, Czerwiński E, Dadgar M, et al. Positronium imaging with the novel multiphoton PET scanner. Sci Adv. 2021;7:eabh4394. doi: https://doi.org/10.1126/sciadv.abh4394.
11. Moskal P, Jasińska B, Stępień E, Bass SD. Positronium in medicine and biology. Nat Rev Phys. 2019;1(9):527–9. doi: https://doi.org/10.1038/s42254-019-0078-7.
12. Goworek T, Ciesielski K, Jasińska B, Wawryszczuk J. Positronium in solids: Analysis of the ortho–para conversion. Chem Phys Lett. 1997;272:91–5. doi: https://doi.org/10.1016/S0009-2614(97)00504-6.
13. Tao SJ. Positronium annihilation in molecular substances. J Chem Phys. 1972;56(11):5499–510. doi: https://doi.org/10.1063/1.1677067.
14. Eldrup M, Lightbody D, Sherwood JN. The temperature dependence of positron lifetimes in solid pivalic acid. Chem Phys. 1981;63:51–8. doi: https://doi.org/10.1016/0301-0104(81)80307-2.
15. Moskal P, Stępień EŁ. Perspectives on translation of positronium imaging into clinics. Front Phys. 2022;10:96986. doi: https://doi.org/10.3389/fphy.2022.969806.
16. Moskal P, Bura Z, Kisielewska D, Shopa RY, Chhokar J, Curceanu C, et al. Performance assessment of the 2γ positronium imaging with total-body PET scanners. EJNMMI Phys. 2020;7:44. doi: https://doi.org/10.1186/s40658-020-00307-w.
17. Moyo S, Moskal P, Stępień EŁ. Feasibility study of positronium application for blood clots structural characteristics. Bio-Algorithms and Med-Systems. 2022;18(1):163–70. doi: https://doi.org/10.2478/bioal-2022-0087.
18. Moskal P, Kubicz E, Grudzień G, Czerwiński E, Dulski K, Leszczyński B, et al. Developing a novel positronium biomarker for cardiac myxoma imaging. EJNMMI Phys. 2023;10:1–12. doi: https://doi.org/10.1186/s40658-023-00543-w.
19. Zgardzińska B, Chołubek G, Jarosz B, Wysogląd K, Gorgol M, Goździuk M, et al. Studies on healthy and neoplastic tissues using positron annihilation lifetime spectroscopy. Sci Rep. 2020;10:11755. doi: https://doi.org/10.1038/s41598-020-68727-3.
20. Fong C, Dong AW, Hill AJ, Boyd BJ, Drummond CJ. PALS: a probe for molecular organisation in self-assembled biomimetic systems. Phys Chem Chem Phys. 2015;17:17527–40. doi: https://doi.org/10.1039/C5CP01921D.
21. Mojsiewicz-Pieńkowska K, Bazar D, Filipecki J, Chamerski K. Investigating the Free Volumes as Nanospaces in Human Stratum Corneum Lipid Bilayers Using Positron Annihilation Lifetime Spectroscopy (PALS). Int J Mol Sci. 2024 Jun 1;25(12):6472. doi: https://doi.org/10.3390/ijms25126472.

22. Liu G, Chen H, Chakka L, Gadzia JE, Jean YC. Applications of positron annihilation to dermatology and skin cancer. Phys Status Solidi Curr Top Solid State Phys. 2007;4(10):3912–5. doi: https://doi.org/10.1002/pssc.200675736.

23. Hugenschmidt C, Ceeh H. The free volume in dried and H2O-loaded biopolymers studied by positron lifetime measurements. J Phys Chem B. 2014;118(31):9356–60. doi: https://doi.org/10.1021/jp504504p.

24. Moyo S, Wróbel A, Leszczyński B, Skalska M, Stępniewski J, Kopeć G, et al. Fresh Paraformaldehyde Preserves Thrombus Biochemistry An ATR – FTIR and PCA Investigation of Pulmonary Artery Thrombi. 2025;1–19. doi: https://doi.org/10.1101/202.11.17.688840.

25. Kiernan JA. Formaldehyde, Formalin, Paraformaldehyde And Glutarahyde: What They Are And what they Do. Hassle-Free: CossMark; 1994;8–13.

26. Echlin P. Low-Temperature Biological Scanning Electron Microscopy. Adv Tech Biol Electron Microsc II. 1978;112:89–12. doi: https://doi.org/10.1007/978-3-642-66809-8_4.2.

27. Chamerski K, Korzekwa W, Filipecki J, Shpotyuk O, Stopa M, Jeleń P, et al. Nanoscale Observation of Dehydration Process in PHEMA Hydrogel Structure. Nanoscale Res Lett. 2017;12:303. doi: https://doi.org/10.1186/s11671-017-2055-3.

28. Consolati G, Nichetti D, Quasso F. Probing the Free Volume in Polymers by Means of Positron Annihilation Lifetime Spectroscopy. Polymers (Basel). 2023;15(14):3128. doi: https://doi.org/10.3390/polym15143128.

29. Wolberg AS, Sang Y. Fibrinogen and Factor XIII in Venous Thrombosis and Thrombus Stability. Arterioscler Thromb Vasc Biol. 2022;42(8):931–41. doi: https://doi.org/10.1161/ATVBAHA.122.317164.

30. Chiu CL, Hecht V, Duong H, Wu B, Tawil B. Permeability of three--dimensional fibrin constructs corresponds to fibrinogen and thrombin concentrations. Biores Open Access. 2012;1(1):34–40. doi: https://doi.org/10.1089/biores.2012.0211.

31. Ramanujam RK, Maksudov F, Litvinov RI, Nagaswami C, Weisel JW, Tutwiler V, et al. Biomechanics, Energetics, and Structural Basis of Rupture in Fibrin Networks. Adv Healthc Mater. 2023;12:2300096. doi: https://doi.org/10.1002/adhm.202300096.

32. Stepien EL, Kwaśniewska M, Rębowska E, Golański J, Drygas W. Modified thrombin formation and fibrinolysis in an ultra-endurance marathon swimmer. Scand J Med Sci Sport. 2017;27(5):567–70. doi: https://doi.org/10.1111/sms.12836.

33. Pretorius E, Briedenhann S, Marx J, Franz RC. Structural changes in the fibrin network of a pretoria family with dysfibrinogenemia: A scanning electron microscopical study. Ultrastruct Pathol. 2006;30(3):167–76. doi: https://doi.org/10.1080/01913120600689772.

34. Piechocka IK, Bacabac RG, Potters M, Mackintosh FC, Koenderink GH. Structural hierarchy governs fibrin gel mechanics. Biophys J. 2010;98(10):2281–9. doi: http://dx.doi.org/10.1016/j.bpj.2010.01.040.

35. Litvinov RI, Weisel JW. Fibrin mechanical properties and their structural origins. Matrix Biol. 2017;60–61:110–23. doi: http://dx.doi.org/10.1016/j.matbio.2016.08.003.

36. Undas A, Stepien E, Tracz W, Szczeklik A. Lipoprotein(a) as a modifier of fibrin clot permeability and susceptibility to lysis. J Thromb Haemost. 2006;4(5):973–5. doi: https://doi.org/10.1111/j.1538-7836.2006.01903.x.

37. Undas A, Ariëns RAS. Fibrin clot structure and function: A role in the pathophysiology of arterial and venous thromboembolic diseases. Arterioscler Thromb Vasc Biol. 2011;31(12):88–99. doi: https://doi.org/10.1161/ATVBAHA.111.230631.

38. Ariëns RAS. Fibrin(ogen) and thrombotic disease. J Thromb Haemost. 2013;11(SUPPL.1):294–305. doi: https://doi.org/10.1111/jth.12229.

39. Kubat K, Kapłon Ł, Moskal P, Stępień E. Calibration of PALS System with CRM Materials for Biomedical Studies. Bio-Algorithms and Med--Systems. 2024;20:35–9. doi: https://doi.org/10.5604/01.3001.0054.9091.

40. Łapkiewicz G, Niedzwiecki S, Moskal P. Developing a Phantom for the Positronium Imaging Evaluation. Acta Phys Pol B, Proc Suppl. 2022;15(4):10–5. doi: https://doi.org/10.5506/APhysPolBSupp.15.4-A4.

41. Dulski K. PALS Avalanche – A new PAL spectra analysis software. Acta Phys Pol A. 2020;137(2):167–70. doi: https://doi.org/10.12693/APhysPolA.137.167.

42. Kansy J. Microcomputer program for analysis of positron annihilation lifetime spectra. Nucl Instmments Methods Phys Res A. 1996;374(96):235–4. doi: https://doi.org/10.1016/0168-9002(96)00075-7.

43. Jean YC, Mallon PE, Schrader DM, editors. Principles and Applications of Positron and Positronium Chemistry. Singapore: World Scientific; 2003. ISBN: 9789812383925.

44. Mogensen OE. Positron Annihilation in Chemistry. Berlin, Heidelberg: Springer; 1995. doi: https://doi.org/10.1007/978-3-642-85123-0.5.

45. Phan-Xuan T, Bogdanova E, Millqvist Fureby A, Fransson J, Terry AE, Kocherbitov V. Hydration-Induced Structural Changes in the Solid State of Protein: A SAXS/WAXS Study on Lysozyme. Langmuir. 2020;36:11745–4. doi: https://doi.org/10.1021/acs.molpharmaceut.0c00351.

46. Hense D, Strube OI. Glutaraldehyde Cross-Linking of Salt-Induced Fibrinogen Hydrogels. ACS Biomater Sci Eng. 2024;10(11):6927–7. doi: https://doi.org/10.1021/acsbiomaterials.4c01412.

47. Migneault I, Dartiguenave C, Bertrand MJ, Waldron KC. Glutaraldehyde: Behavior in aqueous solution, reaction with proteins, and application to enzyme crosslinking. Biotechniques. 2004;37(5):790–802. doi: https://doi.org/10.2144/04375rv01.

48. Nicolle S, Palierne JF. Dehydration effect on the mechanical behaviour of biological soft tissues: Observations on kidney tissues. J Mech Behav Biomed Mater. 2010;3:630–5. doi: https://doi.org/10.1016/j.jmbbm.2010.07.010.

49. Bozzola JJ, Russell LD. Critical point drying for biological specimens. In: Bozzola JJ, Russell LD, editors. Electron Microscopy: Principles and Techniques for Biologists. Sudbury, MA: Jones and Bartlett Publishers; 1999. p. 18–20. ISBN: 9780763701925.

50. Weisel JW. Fibrinogen and fibrin. Adv Protein Chem. 2005;70:247–99. doi: https://doi.org/10.1016/S0065-3233(05)70008-5.

51. Chiu CL, Hecht V, Duong H, Wu B, Tawil B. Permeability of Three -Dimensional Fibrin Constructs. J Biomed Mater Res Part B. 2012;100B:632–9. doi: https://doi.org/10.1089/biores.2012.0211.

52. Wufsus AR, Macera NE, Neeves KB. The Hydraulic Permeability of Blood Clots as a Function of Fibrin and Platelet Density. Biophys J. 2013;104:1812–23. doi: https://doi.org/10.1016/j.bpj.2013.02.055.

53. Ramanujam RK, Maksudov F, Risman RA, Litvinov RI, Weisel JW, Bassani JL, et al. Influence of fibrin network structure on the rupture resistance. Acta Biomater. 2024;174:85–98. doi: https://doi.org/10.1016/j.actbio.2024.10.004.

54. Litvinov RI, Weisel JW. Fibrin mechanical properties and their structural origins. Matrix Biol. 2016;60–61:110–23. doi: https://doi.org/10.1016/j.matbio.2016.08.003.

55. Purohit PK, Litvinov RI, Brown AEX, Discher DE, Weisel JW. Protein unfolding accounts for the unusual mechanical behavior of fibrin networks. Acta Biomater. 2011;7(6):2374–83. doi: http://dx.doi.org/10.1016/j.actbio.2011.02.026.

56. Litvinov RI, Faizullin DA, Zuev YF, Weisel JW. The α-helix to β-sheet transition in stretched and compressed hydrated fibrin clots. Biophys J. 2012;103(5):10207. doi: https://doi.org/10.1016/j.bpj.2012.07.046.

57. Sun J, He H, Zhao K, Cheng W, Li Y, Zhang P, et al. Protein fibers with self-recoverable mechanical properties via dynamic imine chemistry. Nat Commun. 2023;14(1):1–13. doi: https://doi.org/10.1038/s41467-023-41084-1.